ACS APPLIED MATERIALS & INTERFACES

Research Article

www.acsami.org

High Strength Multifunctional Multiwalled Hydrogel Tubes: Ion-Triggered Shape Memory, Antibacterial, and Anti-inflammatory Efficacies

Bing Xu,[†] Yongmao Li,[†] Fei Gao,[†] Xinyun Zhai,[‡] Mengge Sun,[‡] William Lu,[‡] Zhiqiang Cao,[§] and Wenguang Liu*[,†]

[†]School of Materials Science and Engineering, Tianjin Key Laboratory of Composite and Functional Materials, Tianjin University, Tianjin, 300072, China

[‡]Department of Orthopaedics and Traumatology, the University of Hong Kong, Hong Kong, China

[§]Department of Chemical Engineering and Materials Science, Wayne State University, Detroit, Michigan 48202, United States

Supporting Information

ABSTRACT: In this study, ion-responsive hydrogen bonding strengthened hydrogels (termed as PVV) were synthesized by one-pot copolymerization of 2-vinyl-4,6-diamino-1,3,5-triazine (VDT), 1-vinylimidazole (VI), and polyethylene glycol diacrylate. The diaminotriazine−diaminotriazine (DAT−DAT) H-bonding interaction and copolymerization of VI contributed to a notable increase in comprehensive performances including tensile/compressive strength, elasticity, modulus, and fracture energy. In addition, introducing mM levels of zinc ions could further increase the mechanical properties of PVV hydrogels and fix a variety of temporary shapes due to the strong coordination of zinc with imidazole. The release of zinc ions from the hydrogel contributed to an antibacterial effect, without compromising the shape memory effect. Remarkably, a multiwalled hydrogel tube (MWHT) fixed with Zn^{2+} demonstrated much higher flexural strengths and a more sustainable release of zinc ions than the solid hydrogel cylinder (SHC). A Zn^{2+}-fixed MWHT was implanted subcutaneously in rats, and it was found that the Zn^{2+}-fixed MWHT exhibited anti-inflammatory and wound healing efficacies. The reported high strength hydrogel with integrated functions holds potential as a tissue engineering scaffold.

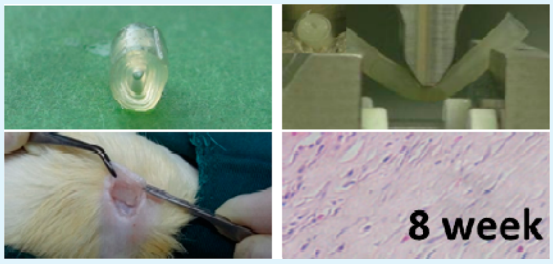

KEYWORDS: *high strength, ion-responsive, multifunctional, implantable, multiwalled hydrogel tubes*

1. INTRODUCTION

Polymer hydrogels are highly hydrated and soft materials, and have been utilized in a variety of biomedical applications including tissue engineering/regenerative medicine scaffolds, drug delivery carriers, and wound filled soft tissue substitutes.[1,2] Nevertheless, conventional hydrogels suffer from weak mechanical properties.[3] To improve the mechanical strength of hydrogels, many approaches have been developed resulting in double network hydrogels,[4,5] nanocomposite hydrogels,[6] macromolecular microsphere composite hydrogels,[7] hydrogen bonding/dipole−dipole reinforced hydrogels,[8−10] sliding ring hydrogels, tetra-PEG hydrogels,[11] and many others.[12−16] Previously we have reported high strength hydrogels based on a hydrogen bonding reinforced mechanism.[17−21] The diaminotriazine−diaminotriazine (DAT−DAT) hydrogen bonding interaction in the hydrogel bulk was shown to significantly enhance both the tensile and compressive strength. However, these hydrogen bonding reinforced hydrogels were low in toughness due to the lack of an effective energy dissipating mechanism. In addition, these hydrogels do not have the antibacterial property, a vital function for potential implantation applications.

It has been widely reported that bacterial infection is a cause of biomaterial implant failure.[22] To combat bacterial infection, antimicrobial hydrogels have emerged using different mechanisms of action against bacterial cells.[23] We are particularly interested in the zinc ion, which is a physiologically important trace element involved in various biological activities and shows strong broad-spectrum antibacterial and anti-inflammatory functions.[24,25] In the body, high dose release of zinc ions should be avoided since this may induce adverse reactions.[26] Typically the release process should be strictly controlled, and a slow and sustained rate is preferred.[27,28] Another important feature for zinc ions is that coordination of zinc ions with imidazole could dramatically increase the mechanical strength of poly(acrylonitrile-*co*-vinyl imidazole) hydrogels and contribute to a shape memory effect.[29] Thus, we expect that the use of zinc ions in hydrogel design can simultaneously improve the mechanical, antimicrobial, and anti-inflamatory properties. In this work, we fabricated multifunctional high strength hydrogels

Received: June 9, 2015
Accepted: July 15, 2015
Published: July 15, 2015

DOI: 10.1021/acsami.5b05074
ACS Appl. Mater. Interfaces 2015, 7, 16865−16872

by one-step copolymerization of 2-vinyl-4,6-diamino-1,3,5-triazine, 1-vinylimidazole, and polyethylene glycol diacrylate. DAT residues in VDT is anticipated to strengthen hydrogels through hydrogen bonding interaction. We examined the effect of zinc ion−imidazole coordination on the toughness and shape memory behavior of the gels; particularly, the difference in mechanical properties and Zn^{2+} release behavior between the Zn^{2+}-fixed multiwalled hydrogel tube (MWHT) and solid hydrogel cylinder (SHC) was investigated. The antibacterial efficacy of Zn^{2+} was evaluated, and the *in vivo* implantation and anti-inflammatory effect of MWHT was studied.

2. EXPERIMENTAL SECTION

2.1. Preparation of P(VDT-*co*-VI) Hydrogels. P(VDT-*co*-VI) hydrogels were synthesized by photoinitiated radical polymerization using PEGDA4K as a cross-linker and IRGACURE-2959 as an initiator. The monomer concentration was fixed at 22%, and the cross-linker was kept at 15 wt % relative to total monomers for all formulations. The hydrogels obtained were named PVV-X, where X represents the VDT/VI weight ratio. To prepare the hydrogel, all ingredients were dissolved in DMSO, and the clear solution was injected into proper molds. Photopolymerization was carried out for 30 min in a cross-linking oven (XL-1000 UV Cross-linker, 365 nm, 2 mW cm^{-2}, Spectronics Corporation, NY, USA). The resulting hydrogels were thoroughly washed with deionized water to remove unreacted monomers and solvent. The molecular structure of the hydrogel is shown in Scheme 1. When hydrogels were treated with zinc ion solutions, they were then denoted by PVV-X-Zn.

Scheme 1. Schematic Molecular Structure of PVV Hydrogels

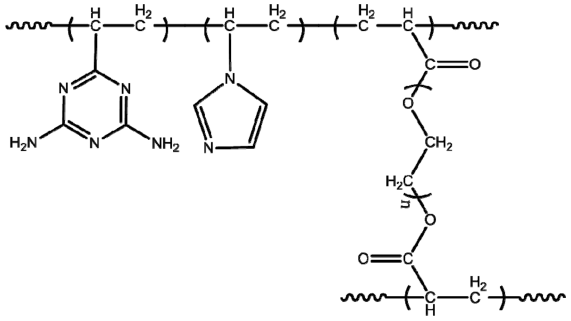

2.2. Characterization of PVV Hydrogels. Equilibrium water content (EWC) for PVV hydrogels was measured at room temperature using a gravimetric method. Disk shaped hydrogels were immersed in PBS, 1 mM, 5 mM, or 10 mM $ZnSO_4$ solutions until reaching the swelling equilibrium. The water on the gel surface was blotted, and the wet weight (m_{wet}) was recorded. Then hydrogels were dried to a constant weight (m_{dry}). The EWC can be calculated by

$$m_{eq} = \frac{m_{wet} - m_{dry}}{m_{wet}} \times 100\% \quad (1)$$

The mechanical properties of hydrogels were measured on a WDW-05 electromechanical tester (Time Group Inc., China) at room temperature. For tensile testing, all samples were cut into rectangular pieces with dimensions of 30 mm × 4 mm × 0.2 mm and the extension rate was set at 100 mm min^{-1}. For compression testing, hydrogels were cut into a cylindrical shape (10 mm in diameter and 8 mm in height) and the compression rate was 10 mm min^{-1}. For tearing testing, hydrogel disks were cut into trouser shaped specimens following the standard of 1/2 size of GBT 529-2008 A (width, 7.5 mm; length, 50 mm; notch length, 20 mm; thickness, 0.5 mm). The extension rate was fixed at 100 mm min^{-1}. The fracture energy was calculated by[9]

$$\Gamma = \frac{F_{ave}}{d} \quad (2)$$

where F_{ave} is the average force during the tear and d is the thickness of the trouser samples. All tests were repeated five times.

2.3. Observation of Shape Memory Effect. The shape memory performance of PVV hydrogels was evaluated at room temperature. The hydrogel sheet was cut into a proper shape, manually transformed into other geometrical shapes, and fixed in 5 mM $ZnSO_4$ solution for 30 min.

2.4. Mechanical Properties of Zn^{2+}-Fixed Multiwalled Hydrogel Tube (MWHT) and Solid Hydrogel Cylinder (SHC). A rectangular hydrogel sheet (60 mm in length and 30 mm in width) was rolled up into a multiwalled tube and fixed in 5 mM $ZnSO_4$. The MWHT samples with dimensions of 10 mm × 8 mm and 8 mm × 20 mm (outer diameter × height) were used for compression and flexural tests, respectively. The dimension of SHC for flexural testing was 8 mm × 20 mm (outer diameter × height). The compression test was performed as described above. A three-point flexural test was performed with a constant span length of 16 mm at 5 mm min^{-1} crosshead speed on an MTS 858 mini Bionix biomechanical testing system. A concentrated load was imposed on the midspan of hydrogel samples at ambient temperature. The flexural strength (σ) was calculated by the formula:[30]

$$\sigma = \frac{8PL}{\pi D^3} \quad (3)$$

where P is the maximum applied load, L is the span of the support points (16 mm), and D is the outer diameter of the hydrogel.

2.5. Zn^{2+} Adsorption on and Release from Hydrogels. The Zn^{2+} adsorption on and release from MWHT or SHC was measured using flame atomic absorption spectrometry (Hitachi 180-80 polarization Zeeman atomic absorption spectrum, Japan). The swollen hydrogels were weighed on a microbalance. Then samples were placed into 10 mL of 5 mM $ZnSO_4$ solution. The adsorption was carried out on a reciprocating shaker at 37 °C. The amount of Zn^{2+} uptake per unit of hydrogel was calculated by[31]

$$q = \frac{(C_0 - C_e) \times V}{m} \quad (4)$$

where C_0 and C_e are the initial and final concentrations of Zn^{2+} in the testing solution, V is the volume of the testing solution, and m is the wet weight of the gel.

To test Zn^{2+} release, Zn^{2+}-adsorbed hydrogels were taken out of the $ZnSO_4$ solution, rinsed with water three times, and immersed in 5 mL of PBS (pH7.4) and incubated at 37 °C on an orbital shaker. Then 1 mL of incubating PBS was taken for testing and replaced with an equal volume of fresh PBS at different time points. The cumulative release of Zn^{2+} per mass of the hydrogel was calculated by the following equation. Each measurement was conducted in triplicate.[32]

$$q' = \frac{V_e \sum_1^{n-1} C_i + V_0 C_n}{m} \quad (5)$$

where V_e is the volume of the replaced medium (V_e = 1 mL), V_0 is the whole volume of the release medium (V_0 = 5 mL), C_n is the concentration of Zn^{2+} in the nth sample, and m represents the wet weight of the original hydrogel.

2.6. Antimicrobial Assays of PVV Hydrogels. A nutrient broth dilution method was used for examining the antibacterial efficacy of hydrogels. Luria−Bertani broth medium (LB) was prepared with deionized water according to the manufacturer's instructions and autoclaved before use for bacterial culture. The bacteria media were diluted to an OD of 0.05 for further assays. To test the antibacterial activity, the Zn^{2+}-adsorbed hydrogel disks were sterilized and placed in 96-well plates. 100 μL of bacteria suspension were inoculated on each hydrogel surface. The culture plates were placed on a shaker at 37 °C, and the OD_{600} readings of the bacteria solution were monitored at a prescribed interval of time. The number of bacteria on the hydrogel was quantified by a spread plate method. Hydrogels were challenged

DOI: 10.1021/acsami.5b05074
ACS Appl. Mater. Interfaces 2015, 7, 16865−16872

Table 1. Mechanical Properties and the EWCs of Hydrogels

sample	$[Zn^{2+}]$ (mM)	EWC (%)	tensile strength (MPa)	Elongation at break (%)	Young's modulus (MPa)	Compressive strength (MPa) at 90%	Fracture Energy (J m^{-2})
PVDT-PEGDA4K	0	73.0 ± 0.1	1.51 ± 0.03	92 ± 12	9.20 ± 1.62	12.99 ± 0.21	908 ± 35
	1	73.1 ± 0.3	1.44 ± 0.07	140 ± 6	8.92 ± 0.08	12.76 ± 0.12	912 ± 21
	5	73.1 ± 0.1	1.43 ± 0.05	148 ± 7	7.50 ± 1.13	12.64 ± 0.26	933 ± 63
	10	72.8 ± 0.2	1.39 ± 0.21	165 ± 22	7.20 ± 0.65	12.47 ± 0.11	967 ± 19
PVV-4	0	78.0 ± 0.1	1.30 ± 0.07	379 ± 9	5.30 ± 1.26	11.34 ± 0.35	1378 ± 105
	1	77.8 ± 0.3	1.42 ± 0.01	327 ± 31	7.61 ± 0.81	12.63 ± 0.18	1399 ± 67
	5	76.5 ± 0.2	1.47 ± 0.01	252 ± 15	19.72 ± 0.80	13.36 ± 0.08	1403 ± 138
	10	76.1 ± 0.2	1.88 ± 0.01	207 ± 10	20.58 ± 1.46	13.63 ± 0.14	1467 ± 29
PVV-2.5	0	79.5 ± 0.2	1.25 ± 0.03	527 ± 54	3.85 ± 0.66	11.12 ± 0.09	1350 ± 28
	1	79.0 ± 0.3	1.76 ± 0.07	393 ± 34	5.85 ± 2.28	13.03 ± 0.21	1352 ± 6
	5	77.3 ± 0.2	1.98 ± 0.05	288 ± 6	11.41 ± 0.39	13.91 ± 0.25	1369 ± 4
	10	77.1 ± 0.2	2.31 ± 0.21	277 ± 11	19.98 ± 1.52	14.06 ± 0.07	1399 ± 89
PVV-1.5	0	80.3 ± 0.4	1.23 ± 0.03	662 ± 29	2.84 ± 0.05	10.64 ± 0.22	1251 ± 62
	1	79.8 ± 0.4	2.03 ± 0.07	511 ± 6	6.98 ± 0.10	13.13 ± 0.25	1275 ± 55
	5	78.0 ± 0.2	2.31 ± 0.08	394 ± 31	12.63 ± 1.01	14.25 ± 0.15	1287 ± 32
	10	77.3 ± 0.1	2.32 ± 0.05	386 ± 27	15.15 ± 0.52	14.48 ± 0.20	1353 ± 68

with bacteria LB solution. At a predetermined time point, microbial suspensions were withdrawn, diluted, and plated on LB agar plates. The plates were incubated for 12 and 24 h at 37 °C. Microbial colonies were formed and counted.

The half maximal inhibitory concentration (IC50) was evaluated using the nutrient broth dilution method. Typically, each sterilized hydrogel was treated by a Zn^{2+} solution at concentrations of 0, 130, 260, 390, 520, and 650 mg/L. Then, the hydrogels were challenged with 100 μL of bacteria suspensions. After 24 h of incubation, the whole dispersions of the samples in the bacterial cultures were analyzed by a spectrophotometer at 600 nm. The IC50 was determined according to a relative cell viability (%)−concentration curve equation. The cell viability is considered to be 100% for hydrogel samples treated by PBS.

2.7. Subcutaneous Implantation. A rectangular hydrogel sheet was rolled into a multiwalled tube and fixed in 5 mM L^{-1} $ZnSO_4$ solution for 12 h. Then the samples were sterilized by 75% alcohol for 48 h and further placed in sterilized PBS for 7 days. The animal experiments were approved by the Animal Ethical Committee of the Academy of Military Medical Sciences, China. Male Sprague−Dawley rats, at the age of 4 weeks, weighing approximately 150 g were involved. Prior to surgery, rats were anesthetized with 8% chloral hydrate solution. The back of the rat was shaved and treated with betadine. Two incisions were made on the left and right side to accommodate the dimensions of the implants. Then two subcutaneous pockets were created by blunt dissection using hemostats. MWHT implants were inserted into the pockets, and then each incision was stitched.

The rats were sacrificed after 3 days and 1, 4, and 8 weeks with an overdose of chloral hydrate. Tissues were collected from each rat surrounding the hydrogels.

Tissue samples were fixed in 4% paraformaldehyde and embedded in paraffin after decalcification by EDTA. They were cut into 8 μm sections and stained with Haematoxylin and Eosin for a histology study.

The quantitative analysis of the inflammatory response was measured by a real time polymerase chain reaction (RT-PCR). Total RNA was isolated from the tissues using a Trizol total RNA extraction kit (Invitrogen, USA) according to the instructions of the manufacturer. RNA (l μg) was reversely transcribed using an All-in-One First-Strand cDNA synthesis kit. The RT-PCR oligonucleotide primers used for rat, iNOS, IL-1β, and MMPs are shown in Table S1. The reactions were set up in duplicates of a 20 μL total volume with 4 μL of each primer (0.2 μM final concentration), 10 μL of Platinum SYBR Green qPCR Super Mix-UDG, and l μL of template. The PCR cycle was set at 95 °C for 10 min, 40 cycles of 95 °C for 15 s, 60 °C for 30 s, and a melt curve analysis was performed at the end of each experiment to verify that a single product per primer pair was amplified. The amplification and analysis were performed using an EP GRADIENT S PCR System (Eppendorf, Germany). The fold increase or decrease was determined relative to a blank control after normalizing using the $2^{-\Delta\Delta CT}$ method.

2.8. Statistical Analysis. Group data were expressed as mean ± SD. The student's t test was used to determine whether data groups differed significantly from each other. Statistical significance was defined as having $P^* < 0.05$.

3. RESULTS AND DISCUSSION

3.1. Characterization and Physicochemical Properties of Hydrogels. In this study, terpolymer hydrogels (PVV) comprising VDT, VI, and PEGDA4K were prepared via photoinitiated random copolymerization (Figure S1). The 4,6-diaminotriazine (DAT) residue of VDT can form intermolecular hydrogen bonding microdomains, thereby remarkably increasing the mechanical strength of the hydrogels.[17] The imidazole groups of VI are able to coordinate with zinc ions and form dynamic cross-linking, further enhancing the gel strength, meanwhile providing a working mechanism to trigger the shape memory effect.[29] PEGDA4K, a hydrophilic cross-linker was used to improve the hydrophilicity of PVDT-based hydrogels. The equilibrium water contents (EWCs) of PVV hydrogels vary between 73% and 80% over the range of experimental feed ratios (Table 1). For the PVDT-PEGDA4K hydrogel in the absence of VI, the tensile strength, elongation at break, Young's moduli, compressive strength, and fracture energy are 1.5 MPa, 92%, 9.2 MPa, 12.9 MPa, and 908 J m^{-2}, respectively. The high mechanical properties are attributed to the established DAT−DAT hydrogen bond strengthening effect.[17] With increased Zn^{2+} concentration, the tensile and compressive strength and moduli slightly declined, and the breaking strain and fracture energy increased moderately (Table 1). The mechanical properties of PVDT-PEGDA4K-based hydrogels are dependent on the solution pH. The pH of $ZnSO_4$ was measured to be 5.5, slightly higher than the pK_a of DAT (5.15).[33] In the presence of the Zn^{2+} solution, DAT−DAT hydrogen bonding tends to break up to a slight degree due to partial protonation of amino groups. This weakened the hydrogen bonding cross-linking, thus decreasing the stiffness and increasing the flexibility. We measured the adsorption of Zn^{2+} in PVDT-PEGDA4K hydrogels. Figure S2 shows that the

DOI: 10.1021/acsami.5b05074
ACS Appl. Mater. Interfaces 2015, 7, 16865−16872

PVDT-PEGDA4K gel can adsorb only a very small quantity of zinc ions. Therefore, zinc ions did not exert a significant effect on the gel mechanical properties. In comparison, when VI was copolymerized into the PVDT-PEGDA4K network without addition of Zn^{2+}, the tensile/compressive strength and moduli of PVV hydrogels decrease to a different extent. However, the fracture energy increased up to 1250−1467 J m^{-2} (Table 1). Moreover, with an increment of VI content, the PVV hydrogels became more hydrophilic and extensible. Taking into account the molecular structure of monomer units, it is possible that VI could form hydrogen bonds with DAT. FTIR and Raman spectroscopies were used to differentiate different hydrogen bonding interactions, but overlapped peaks cannot pinpoint VI-DAT hydrogen bonds. Nevertheless, based on EWCs of hydrogels and variation of macroscopic transparency (Table 1, Figure S3), we found that the PVDT-PEGDA4K hydrogel has lower water adsorption ability and appears translucent. Comparatively, the PVV hydrogel was entirely transparent and exhibited higher EWCs. As demonstrated in our previous study,[20] DAT−DAT hydrogen bonding microdomains were hydrophobic and led to phase separation of the network; while the interaction of VI with DAT can reduce the microphase separation. Thus, the rigid DAT−DAT H-bonding microdomains may be partially dissociated and the formation of weak DAT−VI hydrogen bonding introduces an efficient energy dissipating mechanism, accordingly enhancing the fracture energy and flexibility.

Upon impregnating PVV hydrogels with increased zinc ion concentrations, the tensile/compressive strength and modulus increased with the maximum values reaching 2.3, 14.4, and 20 MPa, respectively. EWCs and elongation at break were consequently lowered. The presence of Zn^{2+} also contributed to further enhancement of fracture energy as shown in Table 1. Among the selected hydrogels, PVV-4 exhibits the maximum fracture energy, 1467 J m^{-2} at 10 mM Zn^{2+}. It is noted that as the concentration of Zn^{2+} is raised above 5 mM, the modulus of the PVV-Zn hydrogel increased significantly. The adsorption experiment indicates that more Zn^{2+} is bound to the PVV hydrogel than the PVDT-PEGDA4K hydrogel (Figure S2). The overall improved mechanical strength of PVV-Zn hydrogels is because that imidazole group had a strong ability to bind the zinc ion, and coordinating mM order of the magnitude of zinc ions with imidazole plays a role in extra physical cross-linking.[29] Furthermore, when external loading was applied, the Zn^{2+}-coordination (physical cross-linkage) serves as a reversible sacrificial bond and ruptures to dissipate energies.[34] Therefore, introducing hydrogen bond and ion-coordinated cross-linking into one network enables one to fabricate hydrogels with high strength and toughness. The mechanical properties of the hydrogel can be easily tuned over a wide range of VDT/VI ratios and zinc ion concentrations.

3.2. Zinc Ions Triggered Shape Memory. As the concentration of Zn^{2+} ion is raised above 5 mM, the PVV hydrogels are increased markedly in Young's modulus (as discussed above). This supports the zinc ion-triggered shape memory phenomenon. The PVV hydrogels were arbitrarily deformed into different temporary shapes such as tetrahedron, pentahedron, and cube and immersed into 5 mM $ZnSO_4$. After 24 h, the temporary shapes could be firmly fixed due to the formation of stable ionic cross-linking (Figure 1). After zinc ions were extracted from the hydrogels with EDTA, the ionic physical cross-linkage was lost. As a result, the hydrogels recovered to their original shape in a few hours.

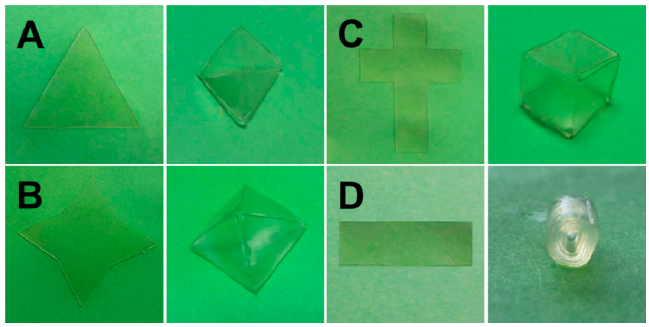

Figure 1. Actual observation of shape memory effect of PVV-2.5 hydrogel. The original triangular, four-angular, cruciform, and rectangular hydrogel sheets were separately curled into a tetrahedron (A), pentahedron (B), cube (C), and multiwalled tube (D), which were fixed in 5 mM $ZnSO_4$ solution.

Intriguingly, we found that when the PVV hydrogel flat sheet was rolled up into to a multiwalled tube, this temporary shape was well fixed in 5 mM Zn^{2+} solution (Figure1D). In contrast, the PVDT-PEGDA4K hydrogel in the absence of VI only formed a loose tubular structure in the same concentration of zinc ions due to the lack of strong Zn^{2+}-imidazole coordination (Figure S4).

To evaluate the memory effect, the PVV-2.5 hydrogel was selected, and its shape fixity ratio (R_f) and shape recovery ratio (R_r) were measured by a reported angle-control method (Figure S5).[35] It was found that both R_f and R_r values reached 100%, indicating Zn^{2+} coordination with imidazole can serve as a reversible physical cross-linking to fix the temporary shape and the temporary shape can return to its permanent shape once zinc ions were released. The shape memory process was fully repeatable.

3.3. Mechanical Property Difference between Zn^{2+}-Fixed MWHTs and SHCs. MWHTs can be firmly fixed with Zn^{2+}, and these MWHTs have a hollow center and ringed cross section (Figure 1D). This is reminiscent of bamboo with a similar inside structure of the stem. It is this unique configuration that contributes to the bamboo's higher flexural strength compared to solid wood due to a more efficient energy dispersion. Hence, it is interesting to compare the flexural strength of MWHTs with that of SHCs in the presence and absence of zinc ions. Figure 2A shows that Zn^{2+}-fixed MWHTs had 54 MPa flexural strength, 1.2-fold that of SHC-Zn. In the absence of Zn^{2+}, both MWHT-PBS (manually fixed with nylon thread) and SHC-PBS showed lower flexural stress; however, MWHT-PBS still has a 1.3-fold increase in flexural strength over SHC-PBS. Figure S6 shows that MWHT did not fracture under the bending load. Likewise, Zn^{2+}-fixed MWHTs and PBS-soaked MWHTs exhibited higher compressive strength than Zn^{2+}-fixed SHCs and PBS-soaked SHCs, respectively (Figure 2B). Flexural strength is very critical for the application of high strength hydrogels as load-bearing soft tissue substitutes.[36] High strength hydrogels have been extensively studied,[37,38] but this property has rarely been explored. Here we demonstrated that a multiwalled configuration can contribute to a considerable increase in flexural strength of a hydrogel, due to its unique geometric structure.

3.4. Antimicrobial Effect of Released Zn^{2+}. Zn^{2+} plays a decisive role in the hydrogel achieving the antibacterial property.[39] Thus, we studied the adsorption capacity of zinc ions in both the MWHT and SHC and the releasing kinetics for

DOI: 10.1021/acsami.5b05074
ACS Appl. Mater. Interfaces 2015, 7, 16865−16872

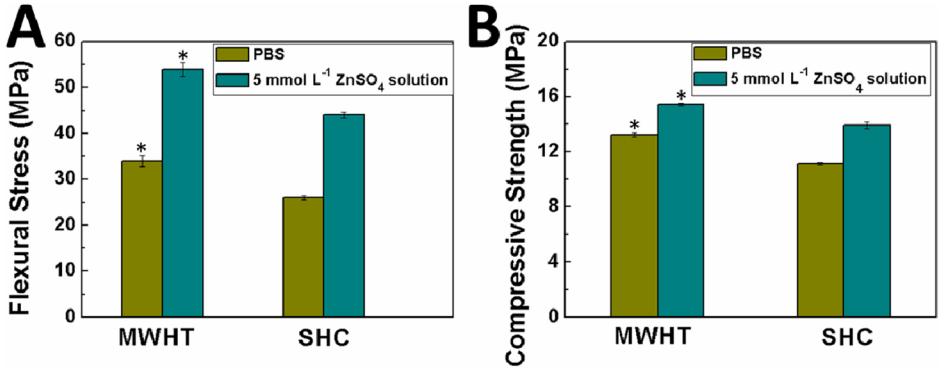

Figure 2. Flexural strength (A) and compressive strength (B) of the PVV-2.5 MWHT and SHC. Asterisks (*) denote significant differences ($P < 0.05$, evaluated by two population student's t test) using SHC as a control.

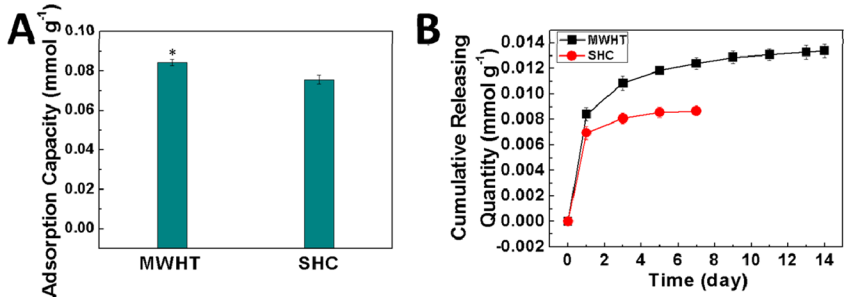

Figure 3. Zn^{2+} adsorption capacity of PVV-2.5 MWHT and SHC (A); Zn^{2+} cumulative release from PVV-2.5-Zn MWHT and SHC in PBS (pH7.4) (B). Asterisks (*) denote significant differences ($P < 0.05$, evaluated by two population student's t test) using SHC as a control.

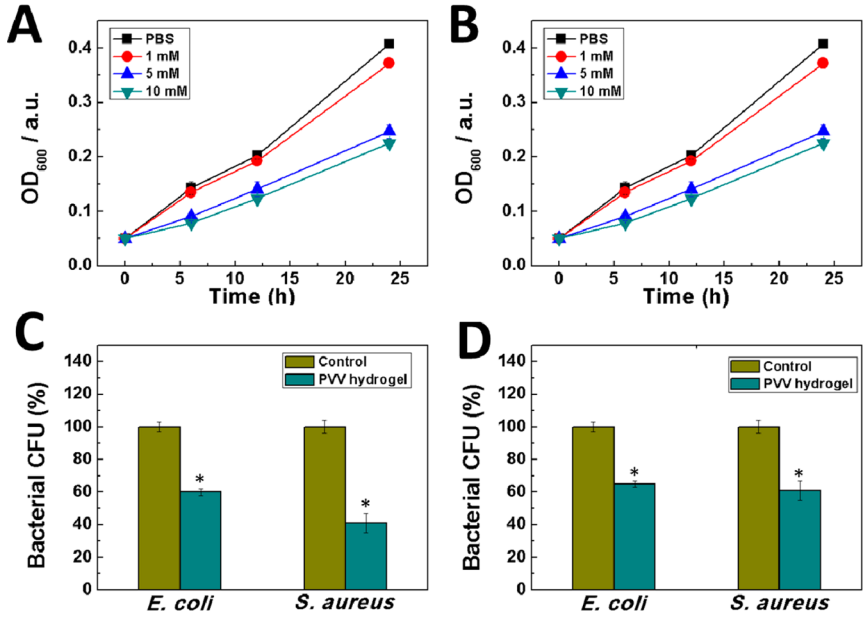

Figure 4. Time-dependent antimicrobial effects of the PVV-2.5 hydrogel against *E. coli* (A) and *S. aureus* (B) bacteria at different Zn^{2+} concentrations. Quantitative antimicrobial results of PVV-2.5-Zn hydrogel treated with 5 mM $ZnSO_4$ solution inoculating bacteria for 12 h (C) and 24 h (D). Asterisks (*) denote significant differences ($P < 0.05$, evaluated by two population student's t test) using PBS-treated group as a control.

zinc. Figure 3A shows that the Zn^{2+} adsorption capacity of MWHTs is 0.084 mmol g^{-1}, slight higher than that of SHCs, 0.075 mmol g^{-1}. A dense network resulted after the Zn^{2+} cross-linkage (Figure S7). Figure 3B shows that there was no difference in the cumulative release of Zn^{2+} between PVV-2.5 SHC and MWHT in PBS for the first 24 h. But after a longer period of time, Zn^{2+} released from the SHC and MWHT reached the maximum value at 5 day and 14 day, respectively. In addition, the MWHT had a 1.5-times higher release capacity than the SHC counterpart. It turns out that 16% and 11.5% Zn^{2+} ions released from the MWHT and SHC, respectively.

To test the antibacterial activity of PVV hydrogels, they were examined utilizing both Gram-positive *Staphylococcus aureus* (*S. aureus*) and Gram-negative *Escherichia coli* (*E. coli*) strains. We monitored the growth of bacteria on the hydrogels immersing in different concentrations of zinc ions. As shown in the Figure

DOI: 10.1021/acsami.5b05074
ACS Appl. Mater. Interfaces 2015, 7, 16865−16872

4A and Figure 4B, upon increasing the Zn^{2+} concentration from 0 to 10 mM, the OD_{600} of the bacterial suspension declined. For the hydrogel treated with 1 mM $ZnSO_4$ solution, the antimicrobial effect is only slightly improved compared with that of the PBS-soaked hydrogel. Further increasing Zn^{2+} to 5 mM and 10 mM resulted in much improved antibacterial activity against both *S. aureus* and *E. coli*. By counting the bacterial colony forming unit (CFU) after culturing the Zn^{2+} treated hydrogel with an LB solution for 12 (Figure 4C) and 24 h (Figure 4D), it was found that 60% *S. aureus* and 40% *E. coli* were killed at 12 h, and 39% *S. aureus* and 35% *E. coli* were killed at 24 h. Figure S8 shows that the IC50 values of the PVV-2.5-Zn hydrogel against *E. coli* and *S. aureus* are 343 and 439 mg/L, respectively. This result indicates that the antibacterial activity of Zn^{2+}-loaded hydrogels is effective, although not very good. It is anticipated that these antimicrobial high strength hydrogels can promisingly be implantable scaffolds, preventing infections with minimized use of antibiotics *in vivo*.

3.5. *In Vitro* Cytotoxicity and *in Vivo* Anti-inflammatory Efficacy of Zinc Ion. Zn^{2+} release shows antimicrobial effects, but can potentially cause cytotoxicity. Thus, L929 cells were cocultured with PVV-2.5-Zn hydrogels treated with different concentrations of zinc ions (Figure 5). With an

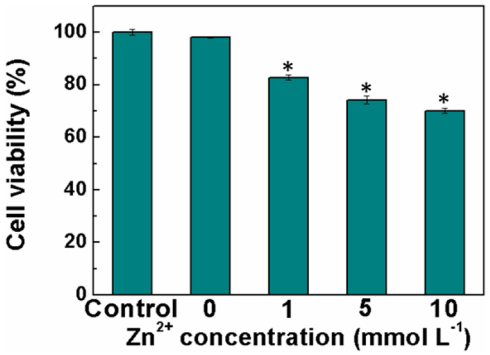

Figure 5. Cell viability of L929 cells cocultured with PVV-2.5 hydrogel treated by different concentrations of zinc ions. Asterisks (*) denote significant differences ($P < 0.05$, evaluated by two population student's *t* test) using nontreated group as a control.

increase in Zn^{2+} concentration, the viability of cells dropped. Good cell viability (up to 76%) can be achieved by treating the gel with 5 mM $ZnSO_4$, which is in agreement with the live–dead assay results (Figure S9).

MWHTs fixed with 5 mM Zn^{2+} were implanted subcutaneously in rats. MWHTs soaked with PBS cannot be "locked" firmly, and the temporary shape was manually maintained prior to surgery and subcutaneously implanted for comparison. The inflammatory response caused by the hydrogels was histologically studied by hematoxylin-eosin (H&E) staining, where the nuclei of the inflammatory cells show purple and normal tissue shows pink (Figure 6). The foreign body reaction and severe inflammatory response were observed at day 3, and there was no notable difference between the Zn^{2+}-fixed and PBS-soaked MWHTs. At 1 week, however, Zn^{2+}-fixed hydrogels significantly decreased the inflammatory response, which was almost gone at 4 weeks. For PBS-soaked MWHTs, a significant inflammatory response prevailed at 1 week, yet a less severe inflammatory response remained at 4 weeks. At 8 weeks, no inflammatory response was observed for both Zn^{2+}-fixed and PBS-soaked hydrogels.

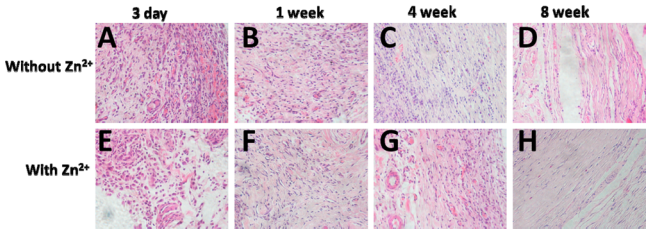

Figure 6. Photomicrographs of HE stained wound histological sections after 3 days and 1, 4, and 8 weeks of subcutaneous implantation of the PVV-2.5 MWHT treated without (A, B, C, and D) and with (E, F, G, and H) $ZnSO_4$ solution.

Macrophages are known to closely contact the muscle and subcutaneous implants within 24 h after implantation.[40] They play a pivotal role in both the inflammatory response and in the foreign body reaction at the tissue level. Chemokines, cytokines, and nitric oxide synthase (iNOS) that can activate the macrophage are good markers of the inflammatory response. MMPs are normally expressed during tissue remodeling and are up-regulated during wound healing.[41] The impact of Zn^{2+}-fixed hydrogels on the expression of IL-1β, iNOS, and MMPs mRNA was studied using RT-PCR. Figure 7 shows that mRNA expression for IL-1β and iNOS induced by both Zn^{2+}-treated and PBS-treated hydrogels was increased sharply at day 3 and remained at a high level at 1 week. At 4 weeks after implantation, a certain degree of inflammatory response still existed. After 8 weeks, there was hardly any mRNA expression. With the addition of Zn^{2+}, the mRNA expression was suppressed at most analyzing time points. This indicates the anti-inflammatory effect of released Zn^{2+}. The mRNA expression for MMP increased with implantation time. At most analyzing time points, the release of Zn^{2+} promoted the expression of MMPs, implying improved wound healing. These mRNA expression results are consistent with those of H&E staining. MWHTs were degradable *in vivo*, and 12% weight loss occurs at 8 weeks (Figure S10A). Along with the degradation, the mechanical property of the implant also deteriorated, but still maintained 1.3 MPa tensile strength and 12 MPa compressive strength thanks to the DAT–DAT hydrogen bonding reinforcement (Figure S10B). Taken together, the degraded MWHT implant was able to avoid the abrupt mechanical failure and reduce the inflammatory response and promote wound healing due to the Zn^{2+} released.

4. CONCLUSION

We constructed a mechanically strong and tough hydrogel with integrated antimicrobial, anti-inflamatory, and wound healing functions through simple one-step copolymerization of 2-vinyl-4,6-diamino-1,3,5-triazine (VDT), 1-vinylimidazole, and polyethylene glycol diacrylate, followed by zinc ion fixation. The diaminotriazine–diaminotriazine (DAT–DAT) hydrogen bonds and copolymerization of VI could significantly increase the comprehensive mechanical properties of the hydrogels, i.e. 1–2 MPa of tensile strength, 11–14 MPa of compressive strength, several hundred percent of break strain, MPa levels of Young's modulus, and over 1000 J m^{-2} of fracture energy. We demonstrated that several mM of zinc ions could further contribute to the enhancement of the mechanical property and the shape memory effect, because of the strong coordination of Zn^{2+} with imidazole. The Zn^{2+}-impregnated hydrogels exhibited an antibacterial property, and a Zn^{2+}-fixed multiwalled

DOI: 10.1021/acsami.5b05074
ACS Appl. Mater. Interfaces 2015, 7, 16865–16872

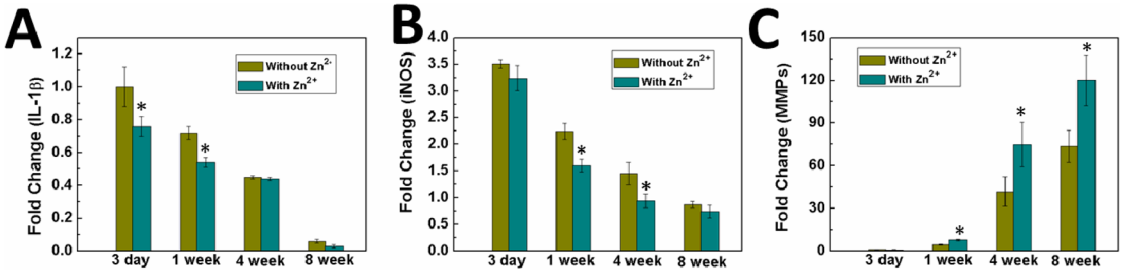

Figure 7. RT-PCR measurement of the expression of IL-1β (A), iNOS (B), and MMPs (C) genes in subcutaneous tissues implanted with MWHT samples. Asterisks (*) denote significant differences ($P < 0.05$, evaluated by two population student's t test) using the implant without Zn^{2+} as a control.

hydrogel tube (MWHT) after subcutaneous implantation showed promoted anti-inflammatory efficacy and wound healing *in vivo*.

■ ASSOCIATED CONTENT

Supporting Information

Supplementary experimental section; FTIR spectra of hydrogels; Zn^{2+} adsorption capacities of hydrogels; photographs of hydrogels; photograph of loose MWHT; Cyclic mechanical experiments; photograph of three-point experiment of MWHT; SEM images of hydrogels; fluorescence micrographs of cells cocultured with hydrogels; weight loss and variation in mechanical properties of MWHT. The Supporting Information is available free of charge on the ACS Publications website at DOI: 10.1021/acsami.5b05074.

■ AUTHOR INFORMATION

Corresponding Author

*E-mail: wgliu@tju.edu.cn.

Notes

The authors declare no competing financial interest.

■ ACKNOWLEDGMENTS

The authors gratefully acknowledge the support for this work from the National Natural Science Foundation of China (Grant Nos. 51173129 and 21274105), National Natural Science Funds for Distinguished Young Scholar (Grant No. 51325305), and Tianjin Municipal Natural Science Foundation (Grants 13ZCZDSY00900, 15JCZD JC38000).

■ REFERENCES

(1) Annabi, N.; Tamayol, A.; Uquillas, J. A.; Akbari, M.; Bertassoni, L. E.; Cha, C.; Camci-Unal, G.; Dokmeci, M. R.; Peppas, N. A.; Khademhosseini, A. 25th Anniversary Article: Rational Design and Applications of Hydrogels in Regenerative Medicine. *Adv. Mater.* **2014**, *26*, 85−123.

(2) Wang, W.; Sun, L.; Zhang, P. F.; Song, J. F.; Liu, W. G. An Anti-inflammatory Cell-Free Collagen/Resveratrol Scaffold for Repairing Osteochondral Defects in Rabbits. *Acta Biomater.* **2014**, *10*, 4983−4995.

(3) Zhao, X. H. Multi-Scale Multi-Mechanism Design of Tough Hydrogels: Building Dissipation into Stretchy Networks. *Soft Matter* **2014**, *10*, 672−687.

(4) Gong, J. P.; Katsuyama, Y.; Kurokawa, T.; Osada, Y. Double-Network Hydrogels with Extremely High Mechanical Strength. *Adv. Mater.* **2003**, *15*, 1155−1158.

(5) Chen, Q.; Zhu, L.; Zhao, C.; Wang, Q. M.; Zheng, J. A. Robust, One-Pot Synthesis of Highly Mechanical and Recoverable Double Network Hydrogels Using Thermoreversible Sol-Gel Polysaccharide. *Adv. Mater.* **2013**, *25*, 4171−4176.

(6) Haraguchi, K.; Takehisa, T. Nanocomposite Hydrogels: A Unique Organic−Inorganic Network Structure with Extraordinary Mechanical, Optical, and Swelling/Deswelling Properties. *Adv. Mater.* **2002**, *14*, 1120−1124.

(7) Huang, T.; Xu, H. G.; Jiao, K. X.; Zhu, L. P.; Brown, H. R.; Wang, H. L. A Novel Hydrogel with High Mechanical Strength: A Macromolecular Microsphere Composite Hydrogel. *Adv. Mater.* **2007**, *19*, 1622−1626.

(8) Bai, T.; Zhang, P.; Han, Y. J.; Liu, Y.; Liu, W. G.; Zhao, X. L.; Lu, W. Construction of An Ultrahigh Strength Hydrogel with Excellent Fatigue Resistance Based on Strong Dipole−Dipole Interaction. *Soft Matter* **2011**, *7*, 2825−2831.

(9) Zhang, Y. Y.; Li, Y. M.; Liu, W. G. Dipole−Dipole and H-Bonding Interactions Significantly Enhance the Multifaceted Mechanical Properties of Thermoresponsive Shape Memory Hydrogels. *Adv. Funct. Mater.* **2015**, *25*, 471−480.

(10) Dai, X. Y.; Zhang, Y. Y.; Gao. L. N.; Wang, W.; Cui, Y. L.; Liu, W. G.; Bai, T. A Mechanically Strong, Highly Stable, Thermoplastic, and Self-Healable Supramolecular Polymer Hydrogel. *Adv. Mater.* **2015**, *27*, 356610.1002/adma.201500534.

(11) Okumura, Y.; Ito, K. olyrotaxane Gel: A Topological Gel by Figure-of-Eight Cross-links. *Adv. Mater.* **2001**, *13*, 485−487.

(12) Sun, J. Y.; Zhao, X. H.; Illeperuma, W. R. K.; Chaudhuri, O.; Oh, K. H.; Mooney, D. J.; Vlassak, J. J.; Suo, Z. G. Highly Stretchable and Tough Hydrogels. *Nature* **2012**, *489*, 133−136.

(13) Guo, M. Y.; Pitet, L. M.; Wyss, H. M.; Vos, M.; Dankers, P. Y.; Meijer, E. W. Tough Stimuli-Responsive Supramolecular Hydrogels with Hydrogen-Bonding Network Junctions. *J. Am. Chem. Soc.* **2014**, *136*, 6969−6977.

(14) Wang, Q.; Hou, R. X.; Cheng, Y. J.; Fu, J. Super-Tough Double-Network Hydrogels Reinforced by Covalently Compositing with Silica-Nanoparticles. *Soft Matter* **2012**, *8*, 6048−6056.

(15) Gao, G. R.; Du, G. L.; Cheng, Y. G.; Fu, J. Tough Nanocomposite Double Network Hydrogels Reinforced with Clay Nanorods Through Covalent Bonding and Reversible Chain Adsorption. *J. Mater. Chem. B* **2014**, *2*, 1539−1548.

(16) Ghoorchian, A.; Simon, J. R.; Bharti, B.; Han, W.; Zhao, X. H.; Chilkoti, A.; López, G. P. Bioinspired Reversibly Cross-linked Hydrogels Comprising Polypeptide Micelles Exhibit Enhanced Mechanical Properties. *Adv. Funct. Mater.* **2015**, *25*, 312210.1002/adfm.201500699.

(17) Tang, L.; Liu, W. G.; Liu, G. P. High-Strength Hydrogels with Integrated Functions of H-Bonding and Thermoresponsive Surface-Mediated Reverse Transfection and Cell Detachment. *Adv. Mater.* **2010**, *22*, 2652−2656.

(18) Tang, L.; Yang, Y.; Bai, T.; Liu, W. G. Robust MeO_2MA/Vinyl-4,6-diamino-1,3,5-triazine Copolymer Hydrogels-Mediated Reverse Gene Transfection and Thermo-Induced Cell Detachment. *Biomaterials* **2011**, *32*, 1943−1949.

(19) Wang, N.; Zhang, J. L.; Sun, L.; Wang, P. Y.; Liu, W. G. Gene-Modified Cell Detachment on Photoresponsive Hydrogels Strengthened Through Hydrogen Bonding. *Acta Biomater.* **2014**, *10*, 2529−2538.

DOI: 10.1021/acsami.5b05074
ACS Appl. Mater. Interfaces 2015, 7, 16865−16872

(20) Wang, N.; Li, Y. M.; Zhang, Y. Y.; Liao, Y.; Liu, W. G. High-Strength Photoresponsive Hydrogels Enable Surface-Mediated Gene Delivery and Light-Induced Reversible Cell Adhesion/Detachment. *Langmuir* **2014**, *30*, 11823−11832.
(21) Zhang, J. L.; Wang, N.; Liu, W. G.; Zhao, X. L.; Lu, W. Intermolecular Hydrogen Bonding Strategy to Fabricate Mechanically Strong Hydrogels with High Elasticity and Fatigue Resistance. *Soft Matter* **2013**, *9*, 6331−6337.
(22) Chen, W.; Liu, Y.; Courtney, H. S.; Bettenga, M.; Agrawal, C. M.; Bumgardner, J. D.; Ong, J. L. In Vitro Anti-Bacterial and Biological Properties of Magnetron Co-Sputtered Silver-Containing Hydroxyapatite Coating. *Biomaterials* **2006**, *27*, 5512−5517.
(23) Alvarez, G. S.; Hélary, C.; Mebert, A. M.; Wang, X. L.; Coradin, T.; Desimone, M. F. Antibiotic-Loaded Silica Nanoparticle−Collagen Composite Hydrogels with Prolonged Antimicrobial Activity for Wound Infection Prevention. *J. Mater. Chem. B* **2014**, *2*, 4660−4670.
(24) Velard, F.; Laurent-Maquin, D.; Braux, J.; Guillaume, C.; Bouthors, S.; Jallot, E.; Nedelec, J. M.; Belaaouaj, A.; Laquerriere, P. The Effect of Zinc on Hydroxyapatite-Mediated Activation of Human Polymorphonuclear Neutrophils and Bone Implant-Associated Acute Inflammation. *Biomaterials* **2010**, *31*, 2001−2009.
(25) Xu, C.; Cai, Y. B.; Ren, C. H.; Gao, J.; Hao, J. H. Zinc-Triggered Hydrogelation of Self-Assembled Small Molecules to Inhibit Bacterial Growth. *Sci. Rep.* **2015**, *5*, 7753.
(26) Yamamoto, A.; Honma, R.; Sumita, M. Cytotoxicity Evaluation of 43 Metal Salts Using Murine Fibroblasts and Osteoblastic Cells. *J. Biomed. Mater. Res.* **1998**, *39*, 331−340.
(27) Miao, S. D.; Cheng, K.; Weng, W. J.; Du, P. Y.; Shen, G.; Han, G. R.; Yan, W. Q.; Zhang, S. Fabrication and Evaluation of Zn Containing Fluoridated Hydroxyapatite Layer with Zn Release Ability. *Acta Biomater.* **2008**, *4*, 441−446.
(28) Malzahn, K.; Jamieson, W. D.; Dröge, M.; Mailänder, V.; Jenkins, A. T. A.; Weiss, C. K.; Landfester, K. Advanced Dextran Based Nanogels for Fighting Staphylococcus Aureus Infections by Sustained Zinc Release. *J. Mater. Chem. B* **2014**, *2*, 2175−2183.
(29) Nan, W. J.; Wang, W.; Gao, H.; Liu, W. G. Fabrication of A Shape Memory Hydrogel Based on Imidazole−Zinc Ion Coordination for Potential Cell-Encapsulating Tubular Scaffold Application. *Soft Matter* **2013**, *9*, 132−137.
(30) Pickles, A. P.; Webber, R. S.; Alderson, K. L.; Neale, P. J.; Evans, K. E. The Effect of the Processing Parameters on the Fabrication of Auxetic Polyethylene. *J. Mater. Sci.* **1995**, *30*, 4059−4068.
(31) Wang, N.; Han, Y. J.; Liu, Y.; Bai, T.; Gao, H.; Zhang, P.; Wang, W.; Liu, W. G. High-Strength Hydrogel as A Reusable Adsorbent of Copper Ions. *J. Hazard. Mater.* **2012**, *213-214*, 258−264.
(32) Li, Y. M.; Xu, B.; Bai, T.; Liu, W. G. Co-delivery of Doxorubicin and Tumor-Suppressing p53 Gene Using A POSS-Based Star-Shaped Polymer for Cancer Therapy. *Biomaterials* **2015**, *55*, 12−23.
(33) Asanuma, H.; Ban, T. S.; Gotoh, S.; Hishiya, T.; Komiyama, M. Precise Recognition of Nucleotides and Their Derivatives through Hydrogen Bonding in Water by Poly(vinyldiaminotriazine). *Supramol. Sci.* **1998**, *5*, 405−410.
(34) Lin, P.; Ma, S. H.; Wang, X. L.; Zhou, F. Molecularly Engineered Dual-Crosslinked Hydrogel with Ultrahigh Mechanical Strength, Toughness, and Good Self-Recovery. *Adv. Mater.* **2015**, *27*, 2054−2059.
(35) Han, Y. J.; Bai, T.; Liu, Y.; Zhai, X. Y.; Liu, W. G. Zinc Ion Uniquely Induced Triple Shape Memory Effect of Dipole-Dipole Reinforced Ultra-High Strength Hydrogels. *Macromol. Rapid Commun.* **2012**, *33*, 225−231.
(36) Roy, R.; Kohles, S. S.; Zaporojan, V.; Peretti, G. M.; Randolph, M. A.; Xu, J. W.; Bonassar, L. J. Analysis of Bending Behavior of Native and Engineered Auricular and Costal Cartilage. *J. Biomed. Mater. Res.* **2004**, *68A*, 597−602.
(37) Lee, J. H.; Park, J.; Park, J. W.; Ahn, H. J.; Jaworski, J.; Jung, J. H. Supramolecular Gels with High Strength by Tuning of Calix[4]arene-Derived Networks. *Nat. Commun.* **2015**, *6*, 6650.
(38) Luo, F.; Sun, T. L.; Nakajima, T.; Kurokawa, T.; Zhao, Y.; Sato, K.; Ihsan, A. B.; Li, X. F.; Guo, H. L.; Gong, J. P. Oppositely Charged Polyelectrolytes Form Tough, Self-Healing, and Rebuildable Hydrogels. *Adv. Mater.* **2015**, *27*, 2722−2727.
(39) Storrie, H.; Stupp, S. I. Cellular Response to Zinc-Containing Organoapatite: An in vitro Study of Proliferation, Alkaline Phosphatase Activity and Biomineralization. *Biomaterials* **2005**, *26*, 5492−5499.
(40) Mantovani, A.; Sica, A.; Sozzani, S.; Allavena, P.; Vecchi, A.; Locati, M. The Chemokine System in Diverse Forms of Macrophage Activation and Polarization. *Trends Immunol.* **2004**, *25*, 677−686.
(41) Tokatlian, T.; Cam, C.; Segura, T. Non-Viral DNA Delivery from Porous Hyaluronic Acid Hydrogels in Mice. *Biomaterials* **2014**, *35*, 825−835.

DOI: 10.1021/acsami.5b05074
ACS Appl. Mater. Interfaces 2015, 7, 16865−16872